PATHOGENS AND GLOBAL HEALTH
2022, VOL. 116, NO. 7, 438–454
https://doi.org/10.1080/20477724.2021.2014235

Taylor & Francis
Taylor & Francis Group

ORIGINAL ARTICLE

Enhancing efficacy of existing antibacterials against selected multiple drug resistant bacteria using cinnamic acid-coated magnetic iron oxide and mesoporous silica nanoparticles

Noor Akbar[a†], Muhammad Kawish[b†], Tooba Jabri[b], Naveed Ahmed Khan[c], Muhammad Raza Shah[b] and Ruqaiyyah Siddiqui[a]

[a]College of Arts and Sciences, American University of Sharjah, University City, Sharjah, UAE; [b]International Centre for Chemical and Biological Sciences, H.e.j. Research Institute of Chemistry, University of Karachi, Karachi, Pakistan; [c]Department of Clinical Sciences, College of Medicine, University of Sharjah, University City, Sharjah, UAE

ABSTRACT

Developing new antibacterial drugs by using traditional ways is insufficient to meet existing challenges; hence, new strategies in the field of antibacterial discovery are necessary. An alternative strategy is to improve the efficacy of currently available antibiotics. Herein, the antibacterial efficacy of drugs (Cefixime, Sulfamethoxazole, and Moxifloxacin) and drug-loaded cinnamic acid-coated magnetic iron oxide and mesoporous silica nanoparticles (NPs) was elucidated versus Gram-negative bacteria (*Pseudomonas aeruginosa, Klebsiella pneumoniae*, neuropathogenic *Escherichia coli* K1 and *Serratia marcescens*) and Gram-positive bacteria (Methicillin-resistant *Staphylococcus aureus* (MRSA), *Streptococcus pyogenes, Streptococcus pneumoniae,* and *Bacillus cereus*). NPs were synthesized by co-precipitation and the Stöber method, and characterized by Fourier transform-infrared spectroscopy, Zetasizer, and Atomic force microscopy. Lactate dehydrogenase (LDH) assays were accomplished to determine drug cytotoxicity against human cells. Spherical NPs in the range of 118–362 nm were successfully synthesized. Antibacterial assays revealed that drugs conjugated with NPs portray enhanced bactericidal efficacies against multiple drug resistant bacteria compared to the drugs alone. Of note, Cefixime-conjugated NPs against *Escherichia coli* K1 and Methicillin- resistant *Staphylococcus aureus*, resulted in the complete eradication of all bacterial isolates tested at significantly lower concentrations compared to the antibiotics alone. Likewise, conjugation of Moxifloxacin resulted in the complete elimination of *E. coli* K1 and MRSA. Of note, nano-formulated drugs presented negligible cytotoxicity against human cells. These results depict potent, and enhanced efficacy of nano-formulated drugs against medically important bacteria and can be used as alternatives to current antibiotics. Future *in vivo* studies and clinical studies are warranted in prospective years to realize these expectations.

KEYWORDS

Antibiotic resistance; multi-drug resistance; magnetic nanoparticles; mic; MBC; cytotoxicity; nanotechnology; drug discovery; infectious diseases

1. Introduction

The declining efficiency of antibacterials in treating common infections has accelerated in recent years, and we are now entering a post-antibiotic era [1]. Supplies of existing antibacterial agents are becoming depleted because of the emergence of drug-resistant microorganisms [2,3]. As a result, multi- and pan drug-resistant bacteria are rapidly emerging and spreading globally, posing a major threat to the public [4–6]. The dramatic rise in antibiotic resistance and the inefficacy of available antibacterial agents have resulted in the unnecessary usage of broad-spectrum antibiotics that has caused the development of further resistance [7]. Furthermore, over the last few years, the industrial pipelines for the discovery of new antibiotics have dried up [8]. Therefore, it is a necessary requirement to develop novel antibacterial agents with improved antibacterial efficacy [9,10]. Given the challenges in discovery of novel antibacterials, an alternative approach is to modify clinically used antibacterials to enhance their efficacy against increasingly resistant bacteria.

Among multiple drug resistance (MDR) bacteria, *Escherichia coli* and Methicillin-resistant *Staphylococcus aureus* (MRSA) cause several infections including gastro-enteritis, meningitis, urinary tract infections (UTIs), skin, respiratory, and other nosocomial infections [11–13]. *Pseudomonas aeruginosa* being a nosocomial pathogen causes 20% of hospital-acquired infections, blood-stream infections and is prevalent in patients with acute leukemia, burn wounds, cystic fibrosis, and organ transplants [14,15]. *Serratia marcescens* colonizes the intensive care unit and causes opportunistic infections [16]. A wide spectrum of invasive infections are caused by *Klebsiella pneumonia* including pneumonia,

CONTACT Naveed Ahmed Khan naveed5438@gmail.com Department of Clinical Sciences, College of Medicine, University of Sharjah, University City, Sharjah 27272, UAE

[†]Both authors contributed equally

meningitis, pyogenic liver abscess, UTIs, bloodstream infection, and intra-abdominal infection etc [17]. *Streptococcus pneumoniae* causes pneumonia in children and has been isolated from patients with purulent pleuritis [18].

At present, Cefixime (453.452 g/mol) is widely used as a broad-spectrum antibiotic with antibacterial effects against *Branhamella catarrhalis, Haemophilus influenza, Streptococcus pneumoniae, Streptococcus pyogenes*, and several *Enterobacteriaceae*. Cefixime is resilient to β-lactamases activity, and is inactive against *P. aeruginosa* and shows minimal activity against *S. aureus* [19,20]. Sulfamethoxazole (253.279 g/mol) is a bacteriostatic antibacterial agent used to treat bronchitis, prostatitis and UTI infections, having effectiveness against *E. coli* and *S. aureus* [21,22]. Similarly, Moxifloxacin (401.431 g/mol) is 8-methoxy fluoroquinolone employed for the treatment of various infections such as nosocomial, upper respiratory tract infections and community-acquired pneumonia. Moxifloxacin is often used as a last resort inhibiting DNA gyrases, topoisomerase II, topoisomerase IV [23]. Given the clinical uses of the aforementioned antibiotics, it is logical to enhance their efficacy. Nanotechnology has been shown to have tremendous potential in targeting bacterial infections [24]. Nanoparticle-based materials have demonstrated profound antibacterial potential *in vitro*. For example, Moxifloxacin-based chitosan nanocomposites augmented the bactericidal activity of Moxifloxacin against *P. aeruginosa, S. aureus*, and several MRSA strains [25]. Similarly, Moxifloxacin conjugation with chitosan-sericin-silver nanocomposite significantly improved the antibacterial properties against *Acinetobacter baumannii, Staphylococcus epidermidis*, and MRSA [26]. Furthermore, Sulfamethoxazole - loaded metal complexes were found to be active against *E. coli* and *S. aureus* [21]. In another study, mesoporous silica-based NPs loaded with ampicillin showed significant antibacterial efficacy against resistant *E. coli* [27]. Ali et al., (2020) reported the antibacterial activity of Ag and Au-conjugated Cefixime NPs [20]. Conjugated Cefixime (CEF- AgNPs and CEF-AuNPs) enhanced the bactericidal effects of Cefixime against *S. aureus* [20]. Similarly, the antibacterial activity of Cefixime was increased upon conjugation with Ag, Nickel, Copper and Zinc oxide NPs [28]. Anwar et al., (2019) reported that conjugation of Hesperidin (Bioflavonoid) with AgNPs enhanced antibacterial activity of Hesperidin [13]. In recent studies, essential oil, *Astragalus verus* Olivier based AgNPs and other Ag nanostructures showed significant antibacterial activity against *S. aureus, B. cereus, S. typhimurium* and *E. coli* [29–31]. Herein, we synthesized Cefixime-loaded magnetic iron oxide NPs and Sulfamethoxazole plus Moxifloxacin-loaded silica-based NPs and elucidated their antibacterial efficacy against various MDR bacteria, in comparison to drugs alone. The findings of this study highlight the potential of utilizing nanoformulations to enhance the efficacy of existing antibiotics used clinically.

2. Materials and methods

The purchased solvents are of high-performance liquid chromatography (HPLC) grade and were acquired from Fisher scientific. Dicyclohexyl carbodiimide (DCC), 4-dimethyl aminopyridine (DMAP), ammonium hydroxide (NH_4OH), Cinnamic acid (CA), 3-aminopropyl silane (APT), ferrous sulfate heptahydrate ($FeSO_4.7H_2O$), Ferric sulfate hexahydrate ($Fe_2(SO_4)_3.6H_2O$), Tetra ethyl orthosilicate (TEOS), cetyl trimethyl ammonium bromide (CTAB), Moxifloxacin (MOX), Sodium borohydride ($NaBH_4$), Sulfamethoxazole (Sul), Naproxen (Nap), Chitosan (CHI), Mannose (Mn) and Cefixime (CEF) were purchased from Sigma Aldrich through local suppliers.

2.1 Preparation of CA-MNPs and CEF-CA-MNPs formulations

Surface modification of magnetic nanoparticles (MNPs) with CA was performed in various steps. Firstly, MNPs were synthesized using co-precipitation technique in accordance with previously published protocol [32]. The synthesized MNPs were then subjected to silane functionalization with APT as previously reported [33]. CA coating at APT-MNPs was conducted as previously reported [29]. Briefly, CA (0.3 g, 2.0 mmol) was added to a flask containing dimethyl formamide (DMF) along with DCC (0.5 g, 2.42 mmol) and DMAP (0.010 g, 0.081 mmol) with constant stirring for 10 min at 60°C. Then, APT-MNPs (0.3 g) were added and the reaction was progressed with constant stirring for 24 h. CA-MNPs were obtained via sequential washing with DMF and stored at 4°C for further analysis. CEF loading onto CA-MNPs was performed by taking various concentrations of CEF (0.5–2 mg/mL) along with the fixed concentration of CA-MNPs (1 mg/mL) and incubated at 200 rpm for 24 h to facilitate the drug uptake. The resulting CEF-CA-MNPs undergo centrifugation and the supernatant containing unreacted drug was analyzed at 261 nm on UV-VIS spectrophotometer. The formulations containing higher loading capacity and narrow size were selected for further analysis.

2.2 Preparation of Mesoporous Silica Nanoparticle (MSN) and APT-MSN

TEOS was used as an alkoxide precursor and CTAB as a surfactant for the synthesis of MSN. The solution of silica was prepared by mixing ammonia solution in 10% ethanol then afterward CTAB (1 g, 2.74 mmol) was added and maintained under constant stirring for 15 min [33]. Then, TEOS (5.0 mL, 25.4 mmol) was

added and the opaque solution was progressed at constant stirring at 60°C for 4 h. The obtained white precipitate was washed successively with water and then washed with methanolic HCl several times for the removal of CTAB. The obtained MSN was dried at room temperature. APT was used as an amino source for the synthesis of APT-MSN. Briefly, MSN (200 mg) was dispersed in methanol at 60°C with constant stirring and then APT (600 µL, 2.56 mmol) was added to keep it on constant stirring for 8 h. The APT-MSN was washed sequentially with Methyl alcohol (CH_3OH), dried at room temperature, and stored at 4°C for further use.

2.3 Preparation of Nap-MSN and Sul-Nap-MSN

Carbodiimide coupling reaction was adopted for the preparation of Nap-MSN. Briefly, Nap (0.4 g, 1.73 mmol) was introduced in a flask containing DMF along with DCC (0.8 g, 3.877 mmol) and DMAP (0.040 g) at 60°C for 5 min. Then, APT-MSN (0.3 g) was added and proceeds under stirring for 24 h. The obtained Nap-MSN was washed several times with DMF and CH_3OH and dried at room temperature. Sul loading within Nap-MSN was performed according to the aforementioned procedure. Briefly, Sul (0.5–2 mg/mL) was taken and keeping the concentration of Nap-MSN (1 mg/mL) and incubated in several ratios for 24 h. The Sul-Nap-MSN was centrifuged and the supernatant was analyzed at 220 nm on UV-VIS spectrophotometer. The formulations containing higher loading capacity and narrow size were selected for further analysis.

2.4 Synthesis of Mn-CHI, Mn-CHI-MSN, and Mox-Mn-CHI-MSN

Mn-CHI was prepared with slight modifications in previously reported protocol [34]. Briefly, 100 mg CHI was allowed to dissolve in a 1% acetic acid solution with the aid of constant stirring for 2 h. Mn (0.5 g) was added to the above solution and allowed the reaction to progress for 1 h. After 1 h, $NaBH_4$ solution (as reductive amination agent) was added drop by drop at pH 5 and allowed to proceed with constant stirring for 24 h. The resulting mixture was neutralized to pH 7 and washed with water several times and dried at room temperature. Mn-CHI-MSN was prepared by incubating Mn-CHI (0.05 g) along with APT-MSN (0.2 g) in water for 10 min with vigorous stirring. The glutaraldehyde (200 µL, 2.11 mmol) was added and the reaction was progressed for 24 h. The resulting Mn-CHI-MSN was washed successively with water and dried at room temperature for further analysis. The aforementioned procedure was adopted for the preparation of Mox-Mn-CHI-MSN. Briefly, Mox (0.5–2 mg/mL) was prepared and incubated with the constant concentration of Mn-CHI-MSN (1 mg/mL) for 24 h. The obtained Mox-Mn-CHI-MSN was centrifuged and the supernatant was analyzed at 291 nm on UV-VIS spectrophotometer. The formulation containing higher loading capacity and narrow size were selected for further analysis.

2.5 Hydrodynamic diameter, polydispersity index (PDI) and morphology

The average sizes of PDI, CA-MNPs, CEF-CA-MNPs, Mn-CHI-MSN, Mox-Mn-CHI-MSN, Nap-MSN, and Sul-Nap-MSN were analyzed from Zetasizer (Zetasizer Nano ZS90 Malvern Instruments, Malvern, UK). Briefly, nano-suspensions (0.1 mg/mL) were transferred to plastic cuvettes with caution to avoid air bubbles. The cuvette was then placed in a spectrometer and the study was conducted at room temperature. The medium viscosity, pressure and refractive index were set at 1.0, 80.4, and 1.33, respectively. CA-MNPs, CEF-CA-MNPs, Mn-CHI-MSN, Mox-Mn-CHI-MSN, Nap-MSN, and Sul-Nap-MSN were further evaluated for surface morphological analysis using Atomic force microscopy (AFM, Agilent 5500, Agilent, USA). The nano-suspension was placed as a drop on mica slide, dried at room temperature and then mounted on a microscope for imaging at non-contact mode.

2.6 Entrapment efficiency determination

The drug loading efficiency of CEF in CA-MNPs was studied by adapting the published protocol [35,36]. Briefly, CEF-CA-MNPs suspension was centrifuged at 12,000 rpm for 15 min to separate CEF-CA-MNPs. After successive dilution of the supernatant, it was analyzed at 261 nm using UV-VIS spectroscopic method. The percentage of drug loading and conjugated efficiency was calculated by using the following equation:

$$\%Drug\ loading = \frac{\text{Amount of drug used} - \text{unloaded drug}}{\text{Amount of drug used}} \times 10$$

2.7 In vitro release study

The release of CEF, Mox, and Sul in buffer solution was evaluated using dialysis method, and with slight modification in a previously reported procedure [37]. Briefly, 10 mg equivalent of CEF-CA-MNPs, Mox-Mn-CHI-MSN, and Sul-Nap-MSN were exposed on the buffer (5 mL; pH 4.0 and pH 7.4) containing 0.1% SDS and loaded into the dialysis bags and fixed at both ends. The bags were then hooked in a flask containing 50 mL of buffer (pH 4.0 and pH 7.4), followed by shaking at 100 rpm at 37°C. At specific time intervals, samples (2 mL) were drawn and replaced with the fresh buffer, and the CEF, Mox, and Sul were quantified at 261, 291 and 220 nm via UV-Vis spectrometer. All experiments

were performed in triplicate using three different batches and data reported as mean values, and the standard deviations were calculated.

2.8 Bacterial isolates used in this study

Several MDR clinical isolates were used in this study, including Gram-negative (*P. aeruginosa, S. marcescens, E. coli* K1 and *K. pneumoniae*) and Gram-positive (*S. pneumoniae, B. cereus, S. pyogenes* and Methicillin-resistant *S. aureus* (MRSA) as depicted (Table 1). All bacteria were isolated from clinical samples. Prior to experimentation, bacteria were cultivated aerobically in nutrient broth (NB) for overnight at 37 °C as described earlier [38,39].

2.9 Antibacterial assays

To determine the bactericidal effects of drugs, NPs, and nanoconjugates against MDR bacteria, antibacterial assays were performed as described earlier [39,40]. Firstly, the optical density of bacterial cultures was adjusted to 0.22 at 595 nm (corresponding to 10^8 colony-forming units (c.f.u) per mL) and enumerated by plating on nutrient agar plates. Based on this, approximately one million bacteria were treated with different drugs, NPs and nano-formulations by incubating at 37°C for 2 h. Following this, cultures were serially diluted (ten-fold) with distilled water and then dispersed onto nutrient agar plates and incubated at 37°C for 24 h. Viable bacterial c.f.u was determined by elucidating the number of bacterial colonies. Bacteria incubated with gentamicin (100 µg/mL) and phosphate buffered saline (PBS) and were taken as positive and negative controls. Methanol (CH_3OH) was used as a solvent control as all the drugs and formulations were dissolved in methanol.

2.10 Minimum inhibitory concentration and minimum bactericidal concentration

Drugs, NPs, and drug-NPs conjugates were tested to find out their minimum inhibitory concentration (MIC) and minimum bactericidal concentration (MBC) against *E. coli* K1 and MRSA using broth microdilution assays [41]. Briefly, drugs, NPs, and their nanoconjugates were serially diluted by two-folds in Muller Hinton broth (MHB) ranging from 1.56 µg/mL – 200 µg/mL. Next, bacterial optical density (OD) was adjusted to 1×10^8 c.f.u/mL (equivalent to 0.5 McFarland's standard). MHB alone and bacteria inoculated in MHB was taken as growth control and sterility control, respectively. The plates were incubated at 37 °C for 24 h. The MIC endpoint is the drugs, NPs and, nanoconjugate's concentration at which no observable growth in the tubes. To confirm the MIC value, the optical turbidity of the tubes was measured before and after incubation.

Following the MIC, 50 µL from all wells with no obvious bacterial growth were plated on nutrient agar plates and the plates were incubated at 37°C for overnight. The MBC endpoint occurs when 99.9% of the bacterial population is demolished at the lowest concentration of drugs, NPs, and nanoconjugates.

Table 1. Bacteria used in this study.

Bacteria	Strain
Streptococcus pyogenes	ATCC 49399 (clinical isolate)
Streptococcus pneumoniae	ATCC 13883 (clinical isolate)
Methicillin-resistant *Staphylococcus aureus*	MTCC 381123 (clinical isolate)
Bacillus cereus	MTCC 131621 (clinical isolate)
Escherichia coli K1	MTCC 710859 (clinical isolate)
Klebsiella pneumoniae	ATCC 13883 (clinical isolate)
Pseudomonas aeruginosa	ATCC 10145 (clinical isolate)
Serratia marcescens	MTTC 13880 (clinical isolate)

2.11 Cell cytotoxicity assay

Host cell cytotoxicity assays were carried out as described, prior [9]. Briefly, assays were performed in a 96-well plate comprising confluent HeLa cells monolayers (P12). Monolayers were treated with 100 µg/mL of different drugs, NPs and nano-formulations and incubated at 37°C for 24 h in the presence of 95% humidity and 5% CO_2. Next day, Triton X-100 (1%) was added to the positive control well and incubated the plate at 37°C for 45–60 min. Next, an equal amount of supernatant (containing LDH) from each well was mixed with equal amount of LDH kit reagents, and cytotoxicity was determined in proportion to LDH released from cervical cancer cells (HeLa ATCC® CCL2™) using a spectrophotometer at 490 nm. Formula for the percent cytotoxicity is as follows:

$$Cytotoxicity(\%) = (samplevalue - negativecontrolvalue)/(positivecontrolvalue - negativecontrolvalue) \times 100$$

As a control, HeLa monolayers were cultivated in RPMI alone (negative control) and total LDH was released by fully lysing HeLa cell lines with 1% of triton X-100 (positive control).

3. Results

3.1 Successful preparation of CA-MNPs and CEF-CA-MNPs formulations

The synthetic scheme of MNPs, APT-MNPs, and CA-MNPs is depicted in Scheme 1. Fourier transformed infrared (FTIR) spectra of MNPs, APT-MNPs, and CA-MNPs are presented in (Figure 1(a)). The MNPs showed well-defined peaks at 639.3 cm^{-1}, 1643 $cm^{-1,}$ and 3387 cm^{-1}. The appearance at 639.3 cm^{-1} is due to

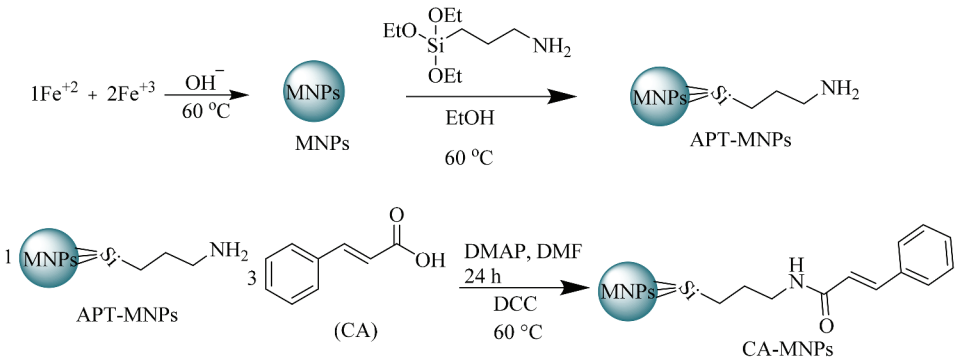

Scheme 1. Synthetic scheme of MNPs, APT-MNPs and CA-MNPs.

Fe-O stretch. Moreover, the peaks at 1643 cm $^{-1}$ and 3387 cm $^{-1}$ are due to the bending vibration of absorbed water and O-H stretching, respectively, [42]. The Si-O stretching bands at 1115 cm^{-1} and 1016 cm^{-1} in addition, NH_2 bending and stretching vibrations around 3472 cm^{-1} and 1635.5 cm^{-1} was indicative for silane modification onto MNPs [43]. CA alone is showing broad absorption around 3200 to 2000 cm^{-1} indicating the presence of —COOH moiety. Furthermore, (C = O) and (C = C) absorptions are also observed at 1700 and 1644 cm^{-1} [44]. The broad band of CA diminishes when it is functionalized onto APT-MNPs (Figure 1(a)). The (N-H) stretching of amide was observed at 3395 cm^{-1} in combination with aliphatic and aromatic (C-H) around 2939 cm^{-1} and 2863 cm^{-1} respectively. The symmetric vibrational of – C = O of amide and asymmetric C-O stretching from – COOH was observed at 1656 cm^{-1} 1244 cm^{-1} respectively for CA-MNPs formation. The CEF molecule showed characteristic stretching at 1777 cm^{-1}, 1662 cm^{-1} and 1595 cm^{-1} corresponding to (C = O, carboxylic acid), β-lactam (N-H) and C = N respectively [45]. These bands were shifted to 1724 cm^{-1}, 1656 cm^{-1} and 1511 cm^{-1} (Figure 1(b)) respectively. It is shown from FTIR comparison that the CEF absorption onto CA-MNPs occured through amide, carboxylic, C = N groups via non-covalent interactions.

3.2 Preparation of Nap-MSN and Sul-Nap-MSN

The development of Nap-MSN was processed in several steps as depicted in Scheme 2. The FTIR spectra of synthesized MSN, APT-MSN, and Nap-MSN are depicted in (Figure 2(a)). Synthesized MSN showed characteristic absorptions around 3369 cm^{-1}, 1619 cm^{-1}, 1232 cm^{-1}, and 1059 cm^{-1} corresponding to OH (stretching and bending), and Si-O groups [45]. When functionalized with APT (APT-MSN) peaks appears at 3220 cm^{-1}, 1551 cm^{-1}, and 2928 cm^{-1}attributes to N-H (stretching and bending) and C-H (stretching) vibrations [46]. Surface modification with Nap (Nap-MSN) was confirmed by peaks around 3335 cm^{-1}, 2854 cm^{-1}, 1436 cm^{-1}, and 1632 cm^{-1} corresponds to N-H (stretching), C-H (stretching and bending) and C = O (amide), respectively. In the spectra of Sul-Nap-MSN, the peaks related to Sul were observed at 1626 cm^{-1}, 1551 cm^{-1}, 1437 cm^{-1}, 805 cm^{-1}, and 621 cm^{-1} (Figure 2(b)) were assigned to N-H (bending), C = N (stretching), C-H (bending) C-N, and C-H (bending), respectively [47]. The appearance of this peak confirmed that Sul was loaded onto synthesized mesoporous nanocomposites.

3.3 Synthesis of Mn-CHI, Mn-CHI-MSN, and Mox-Mn-CHI-MSN

FTIR analysis was conducted in order to elucidate possible interaction between Mn and CHI (Figure 3(a)). CHI showed absorption at 1601 cm^{-1} which is attributed to the amino group and 1360 cm^{-1} corresponded to C-H vibration. Moreover, the absorption band at 1109 cm^{-1} corresponds to asymmetric stretching of C-O-C, and another broad band of 3425 cm^{-1} was observed which was assigned as N-H (symmetric stretching), respectively. In case of Mn-CHI bending of amines was observed at 1563 cm^{-1} and C = N peak at 1443 cm^{-1} showed the formation of Schiff base between mannose and terminated amines. Moreover, an intense broad -OH stretch of Mn was observed at 3218 cm^{-1} and C-O absorption at 1052 cm^{-1} confirmed the presence of excessive -OH groups in Mn-CHI respectively [34]. The surface coating of Mn-CHI on MSN was confirmed by absorptions that appeared at 3383 cm^{-1}, 1560 cm^{-1}, 1407 cm^{-1}, 1239 cm^{-1}, and 1069 cm^{-1} which were assigned to OH (stretching), N-H (stretching), C = N (stretching) and S-O (stretching) vibrations. These vibrations showed that Mn-CHI was coated on MSN via Schiff base pathway. In case of Mox-Mn-CHI-MSN, the peaks of Mox appeared at 1714 cm^{-1}, 1578 $cm^{-1,}$ and 1457 cm^{-1} corresponded to C = O (stretching), C = C (stretching), and C-N (stretching) (Figure 3(b)), respectively [48]. The development of these peaks represents the loading of Mox within the developed mesoporous structure.

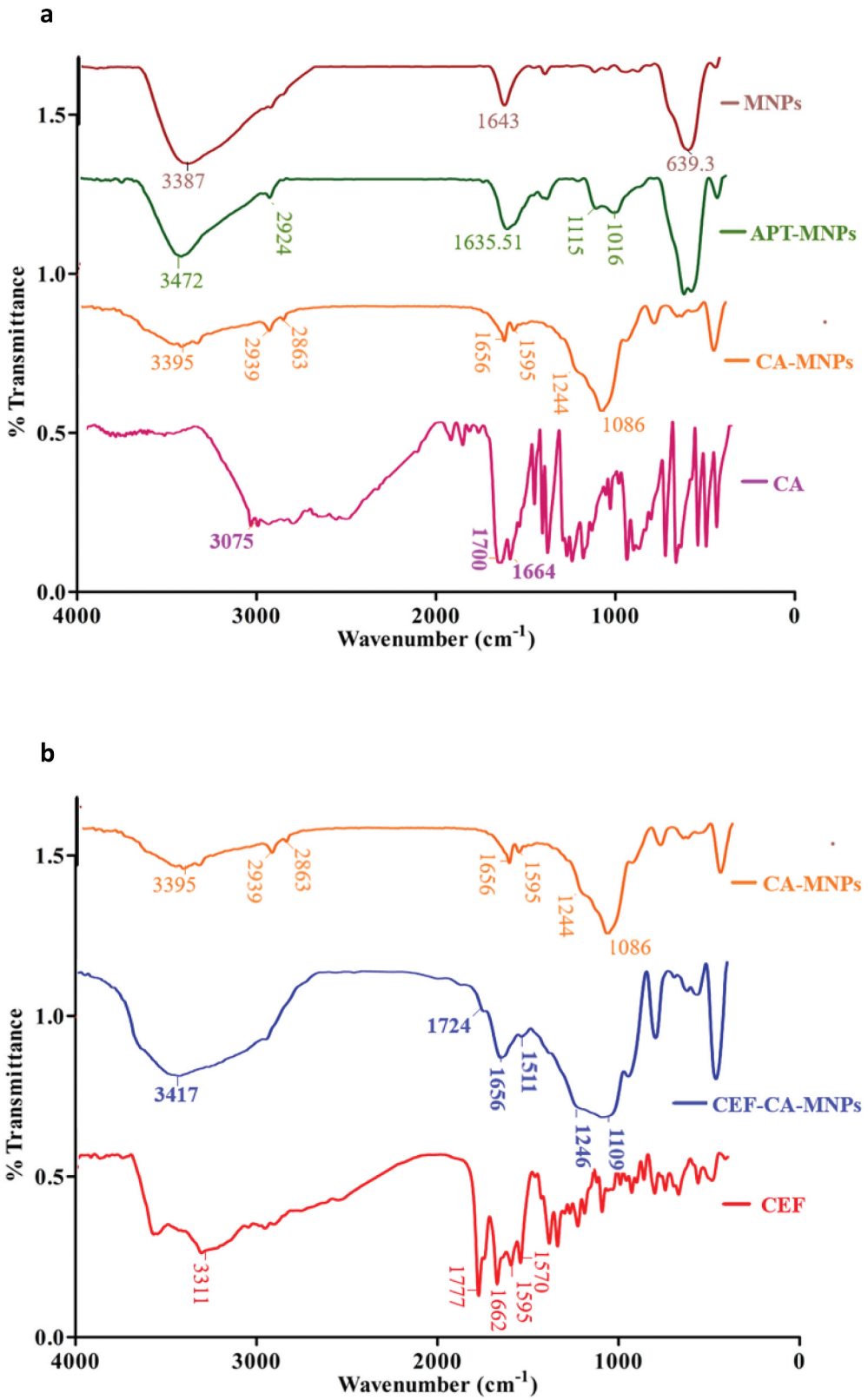

Figure 1. **A**. FTIR spectra of MNPs, APT-MNPs, CA and CA-MNPs, **b**. FTIR spectra of CA-MNPs, CEF and CEF-CA-MNPs.

3.4 Hydrodynamic diameter, polydispersity index (PDI), and morphology

The average size of CA-MNPs, CEF-CA-MNPs, Nap-MSN, Sul-Nap-MSN, Mn-CHI-MSN, and Mox-Mn-CHI-MSN are depicted in (Table 2), respectively. The increment in size Sul-Nap-MSN and Mox-Mn-CHI-MSN may be due to incorporation of drug within cavities Nap-MSN and Mn-CHI-MSN respectively [42]. Decrease in size occurred in case of CEF-CA-MNPs as compared to CA-MNPs, which may be due to decrease in aggregation, as MNPs tend to aggregate

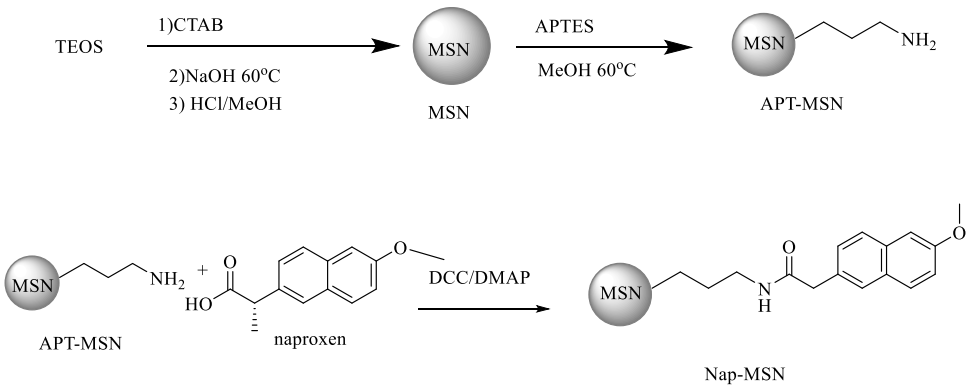

Scheme 2. Synthetic scheme of MSN, APT-MSN and Nap-MSN.

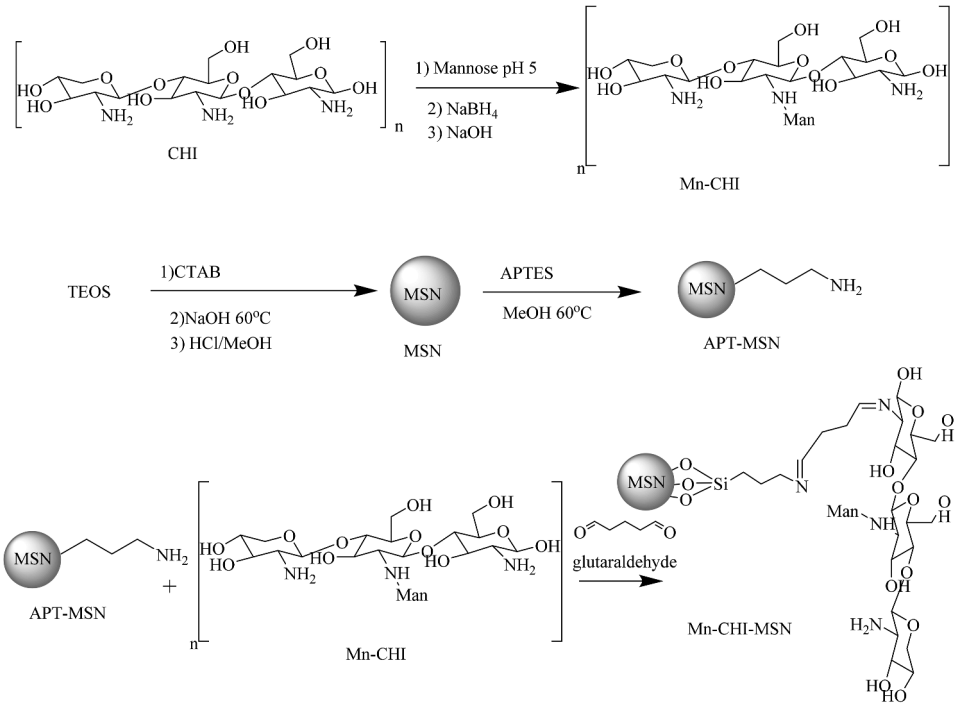

Scheme 3. Synthetic scheme of Mn-CHI, MSN, APT-MSN and Mn-CHI-MSN.

rapidly due to magnetic dipoles [49]. The PDI suggested the uniform dispersion of nanosuspension, as a PDI value of more than 0.5 indicates size broadening of NPs [50]. The PDI values of CA-MNPs, CEF-CA-MNPs, Nap-MSN, Sul-Nap-MSN, Mn-CHI-MSN, and Mox-Mn-CHI-MSN are represented in Table 2. The experimental PDI value suggested that the drug loaded formulation showed more uniform dispersion in comparison to unloaded analogues, suggesting higher colloidal stability nano-formulations. As NPs based formulations are increasingly utilized for site-specific delivery, literature analysis showed that NPs less than 1000 nm may easily permeate the biological barriers to transport drugs at the desired site of action in increased amount [51]. NPs had nearly spherical morphology, regardless of drug inclusion which showed stability of these nanostructures, as shown by AFM (Figure 4), consolidating the findings of our study.

3.5 Drug entrapment efficiency

The loading capacity and controlled release of drugs are generally related to the chemical nature of the drug and to the nature of interaction with the carriers [52]. CEF is a weekly acidic hydrophobic molecule with pKa 3.69 (-COOH), respectively. The entrapment efficiency of CEF within CA-MNPs was found to be 91 ± 0.5%, respectively. The significant adsorption of CEF may be attributed to the increased surface hydrophobicity in the form of CA onto the surface of MNPs. Furthermore, it was

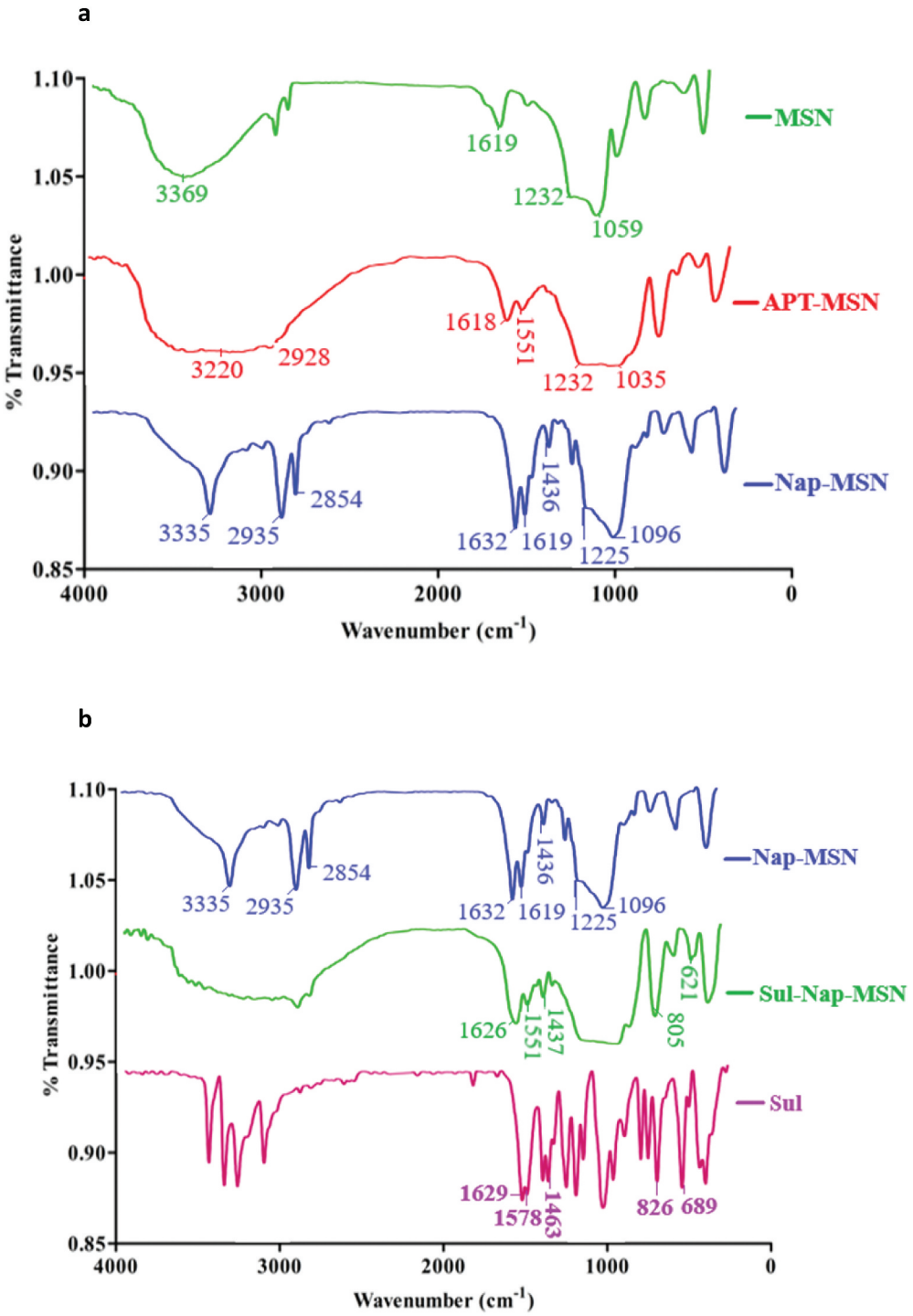

Figure 2. **A**. FTIR spectra of MSN, APT-MSN and Nap-MSN. **b**. FTIR spectra Nap-MSN, Sul-Nap-MSN and Sul.

shown through FTIR that CEF involved in chelation with MNPs, which is another factor for higher drug absorption [32].

The adsorption of drug using the solvent method is the most experimented method for the drug encapsulation within nanostructures [53]. Typically, the drug was first introduced to a nanosuspension of desired concentration and then equilibrium was favored toward the drug loaded formulation in addition, the size of the pores promotes mobility of drug with NPs [54]. In the current study, the encapsulation efficiency of Sul within Nap-MSN was found to be 75.9 ± 1.5% and Mox within Mn-CHI-MSN was found to be 62.0 ± 2.5%, respectively. The higher amount of loading may be attributed to the hydrophobic cavities of MSN with favors the encapsulation of hydrophobic drugs [55].

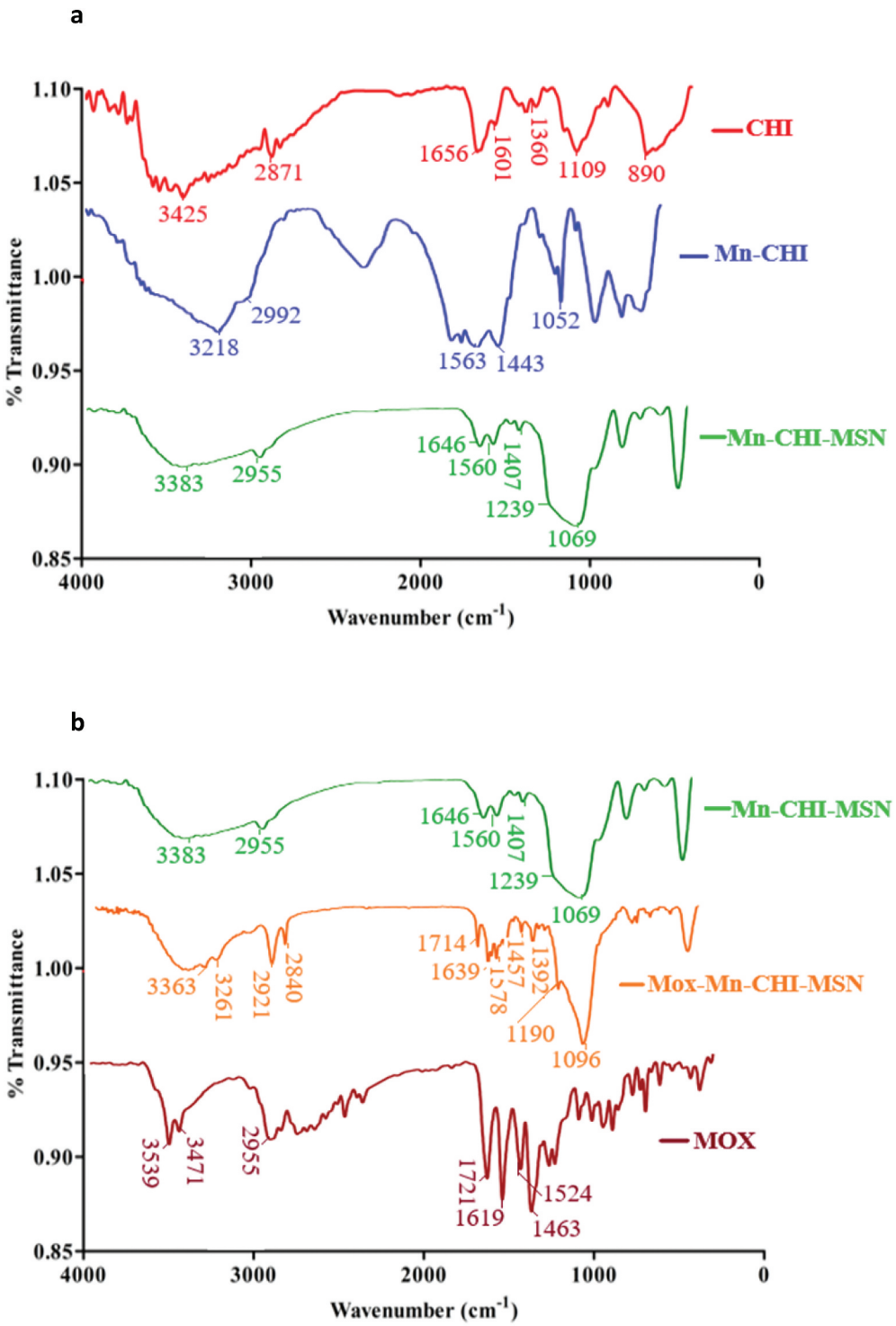

Figure 3. **A**. FTIR spectra of CHI, Mn-CHI and Mn-CHI-MSN. **b**. FTIR spectra of Mn-CHI-MSN, Mox-Mn-CHI-MSN and Mox.

Table 2. Average size and PDI of drug loaded CEF-CA-MNPs, Sul-Nap-MSN, Mox-Mn-CHI-MSN, and vacant CA-MNPs, Nap-MSN, Mn-CHI-MSN nanocomposites.

Nanoparticles	Average Size (nm)	PDI
CA-MNPs	362 ± 40.9	0.46 ± 0.010
CEF-CA-MNPs	157.3 ± 4.60	0.16 ± 0.065
Nap-MSN	255.3 ± 15.9	0.245 ± 0.076
Sul-Nap-MSN	328.9 ± 21.8	0.060 ± 0.040
Mn-CHI-MSN	118.7 ± 5.10	0.294 ± 0.057
Mox-Mn-CHI-MSN	159.0 ± 1.55	0.142 ± 0.053

3.6 In vitro *release of CEF from CA-MNPs*

In vitro release study of CEF from CA-MNPs, Sul from Nap-MSN, and Mox form Mn-CHI-MSN were performed under weakly acidic (pH 4.0) and blood physiological conditions (pH 7.4) under ambient conditions (Figure 5). The higher release of drug in case of CEF-CA-MNPs was observed at 4 h so that 16 ± 0.43% was released at pH 4.0 and 22.3 ± 0.54% at pH 7.4, and then

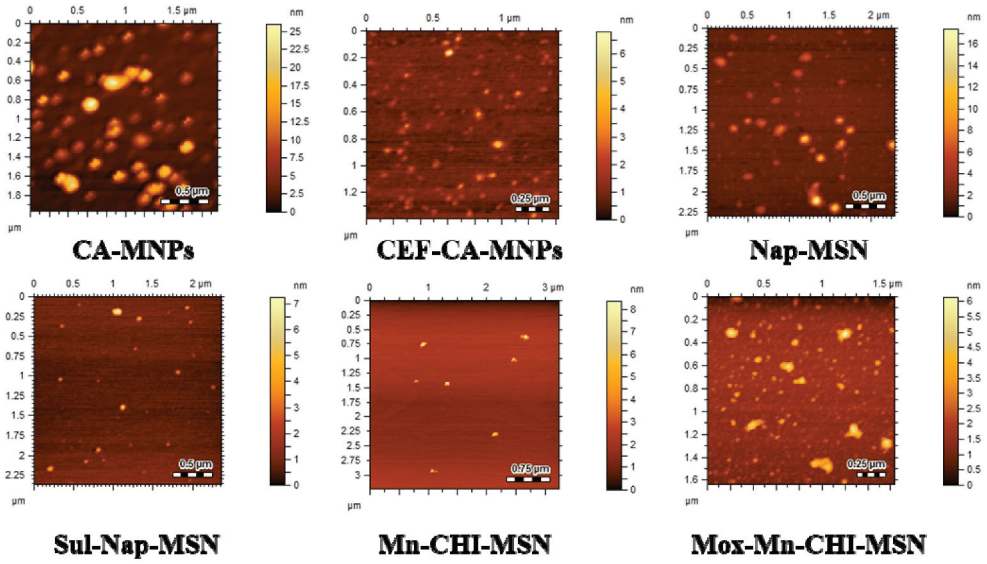

Figure 4. Atomic force microscopic images CA-MNPs, CEF-CA-MNPs, Na-MSN, Sul-Nap-MSN, Mn-CHI-MSN and Mox-Mn-CHI-MSN showing nearly spherical morphology.

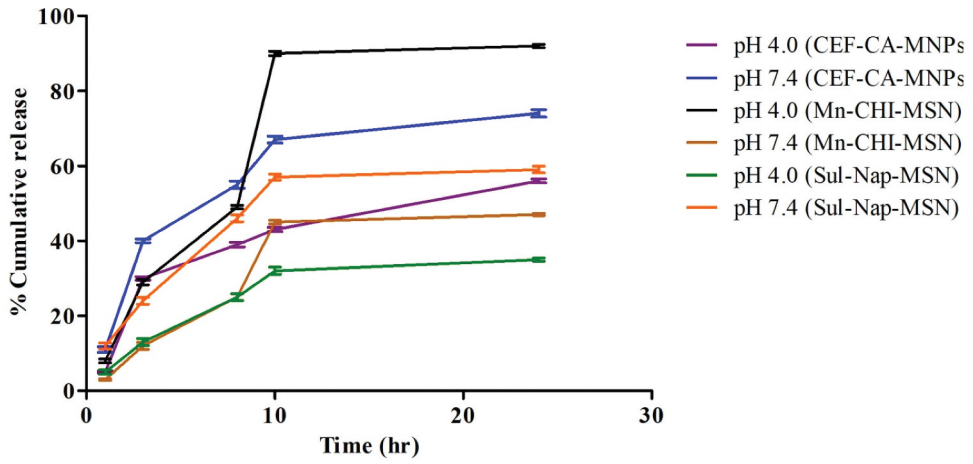

Figure 5. Cumulative release profile of CEF-CA-MNPs, Sul-Nap-MSN and Mox-Mn-CHI-MSN at pH 4.0 and pH 7.4.

sustained this profile till 24 h. Moreover, the higher cumulative release of 74.0 ± 0.95% at pH 7.4 in comparison with pH 4.0 (54 ± 0.54%) revealed the stability of CEF-CA-MNPs in acidic conditions, potentially suggesting that similar resistance might happen in the acidic environment of the stomach. In case of Sul-Nap-MSN, the maximum release of 22 ± 0.90% at pH 7.4 was observed in comparison with 12 ± 0.93% at pH 4.0 after 8 h and then maintaining sustained drug concentration until 24 h. Moreover, a higher cumulative release of 59 ± 0.90% was observed at pH 7.4 in comparison with 35 ± 0.45% at pH 4.0 suggesting the gastric stability of the developed formulation [56]. Furthermore, an increased amount of cumulative release was observed at pH 4.0 in case of Mox-Mn-CHI-MSN was found to be 92 ± 0.48% in contrast with 47 ± 0.32 at pH 7.4 (Figure 5), respectively. In addition, the maximum release of 41 ± 0.85% and 20 ± 0.49% at pH 4.0 and 7.4 was observed after 10 h suggesting that protonation of chitosan terminal amines occurs at acidic pH, which triggers the drug release [57].

3.7 Magnetic iron oxide and silica-based nanoparticles presented important bactericidal efficacies against pathogenic bacteria

All the drugs alone (Cefixime, Sulfamethoxazole, and Moxifloxacin), NPs and their nanoconjugates were evaluated for their antibacterial activities. The results from antibacterial assays have shown that all the treatments (drugs, NPs, and drug-NPs conjugates) presented important antibacterial properties against *P. aeruginosa* when compared with the solvent control ($P \leq 0.05$, using student's T-test, two-tailed distribution) (Figure 6(a)). When drug-NPs conjugates were compared with drugs and NPs alone, Cefixime conjugated CA-MNP (CEF-CA-

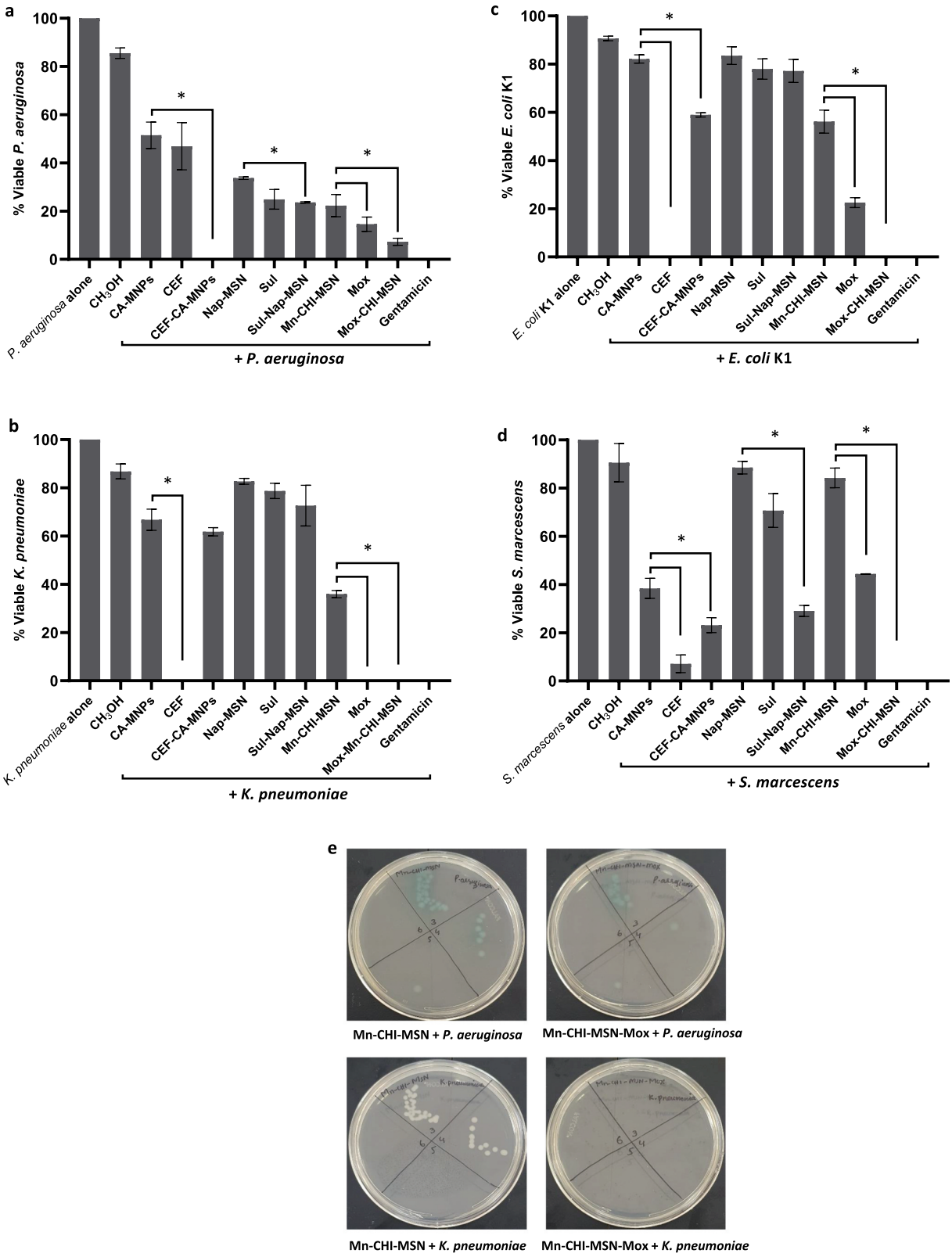

Figure 6. Magnetic iron oxide and silica based NPs loaded with various drugs presented essential antibacterial activity against Gram-negative pathogenic bacteria. Briefly, bacteria (1×10^6) were incubated with different drugs conjugated with ZnO-NPs and nanoparticle alone at 37°C for 2 h. Next, the cultures were ten-fold serially diluted and plated onto the nutrient agar plates and the plates were incubated for overnight at 37°C and counted the viable bacterial colonies on the following day. For negative control, bacteria were incubated in PBS alone whereas for positive control gentamicin (100 µg/mL) was used. The data are expressed as the means ± standard errors from several independent experiments performed in duplicate where (*) represent when $P \leq 0.05$.

MNP) showed significant antibacterial effects (100%) against *P. aeruginosa* (P ≤ 0.05) (Figure 6(a)). Similar effects were observed when Sulfamethoxazole conjugated with Nap-MSN (Sul-Nap-MSN), while in case of Moxifloxacin, the drug alone as well as its conjugate counterpart exhibited remarkable bactericidal activity (93%) against *P. aeruginosa* (Figure 6(a)). In the case of *K. pneumoniae*, all compounds, NPs and drug-NPs counterparts showed noteworthy bacterial killing effects except Sulfamethoxazole, Nap-MSN and Sul-Nap-MSN. Furthermore, Cefixime, Moxifloxacin drug alone and Mox-Mn-CHI-MSN presented exceptional antibacterial activity killing 100% bacteria when compared to the NPs alone (i.e. Mn-CHI-MSN) (P ≤ 0.05) (Figure 6(b)). Similarly, Cefixime, Moxifloxacin drugs, and their NPs homologues exhibited remarkable bactericidal activity. Cefixime alone and Mox-Mn-CHI-MSN abolished 100% *E. coli* K1, whereas CEF-CA-MNP and Moxifloxacin eradicated 41% and 78% bacterial population (P ≤ 0.05) (Figure 6(c)). Sulfamethoxazole and its nanoconjugated equivalent did not show any effect against *E. coli* K1. Against *S. marcescens*, when compared with solvent control, all the treatments except Nap-MSN and Mn-CHI-MSN showed notable antibacterial properties (P ≤ 0.05) (Figure 6(d)). Moreover, CEF and CEF-CA-MNP revealed significant bactericidal activity destroyed 93% and 77% *S. marcescens* (P ≤ 0.05) (Figure 6(d)). Mox and Mox-Mn-CHI-MSN demonstrated prominent antibacterial effects demolished 56% and 100% bacteria while Sul-Nap-MSN had 71% bacterial killing properties (P ≤ 0.05) (Figure 6(d,e)).

Among Gram-positive bacteria, all drugs and drug-NPs revealed noticeable bactericidal activities against *S. pneumoniae* (P ≤ 0.05) (Figure 7(a)) when compared to the NPs alone. Likewise, all the treatments except CA-MNP and Nap-MSN showed substantial antibacterial properties when compared to the solvent control (i.e. MeOH) (P ≤ 0.05) (Figure 7(a)). When tested against MRSA, similar effects were observed where all the treatments except CA-MNP and Nap-MSN revealed important antibacterial properties (P ≤ 0.05) (Figure 7(b)) while the NPs conjugation further enhanced the bactericidal effects of the drugs when compared to the drugs alone (P ≤ 0.05) (Figure 7(b)). In particular, the bactericidal effects of CEF and Sul was tremendously augmented from 51% and 46% to 100% and 68%, respectively, while both Mox and Mox-Mn-CHI-MSN abolished 100% MRSA (P ≤ 0.05) (Figure 7(b)). In case of *B. cereus*, CEF and Mox alone and upon conjugation with NPs revealed remarkable antibacterial activity (P ≤ 0.05) (Figure 7(c)). CEF and CEF-CA-MNP reduced the viability of *B. cereus* up to 14% and 33%, respectively, while Sulfamethoxazole and its NPs analog did not show bacterial killing effects. Finally, when tested against *S. pyogenes*, CEF, Mox, and Mox-Mn-CHI-MSN showed 100% bacterial killing effects (P ≤ 0.05) (Figure 7(d,e)). In addition, Mn-CHI-MSN alone displayed significant bactericidal activity while Sul and Sul-Nap-MSN failed to show any effects (P ≤ 0.05) (Figure 7(d,e)).

The MIC and MBC values of CEF, Sulp, Mox, and their conjugated NPs are summarized in Table. 3. The overall findings revealed that drugs and drug-loaded NPs showed considerable bactericidal effects against the MDR clinical isolates.

3.8 Drugs and drug-NPs conjugates demonstrated marginal cytotoxicity

LDH assays were accomplished to investigate the cytotoxicity of drugs, NPs and drug-NPs on human cells. Upon an overnight incubation, the results depicted that most of the drugs and drug-NPs demonstrated low cytotoxicity (Figure 8). The NPs CA-MNP, and Mn-CHI-MSN showed 38% and 43% cytotoxicity toward HeLa cell lines and rest of all the treatments had minimal cytotoxic activity.

4. Discussion

The advent of multidrug-resistant bacterial infections has resulted in developing alternative methods to overcome antibacterial resistance [58]. The overuse/misuse of antibiotics, as well as a lack of new drug development by the pharmaceutical sector due to limited economic incentives and demanding regulatory requirements, have all been blamed for the antibiotic resistance crisis [59–61]. As a result, there is a persistent need to discover innovative, long-lasting, and efficient chemotherapeutics for infectious diseases. Nanotechnology has proven to be an effective tool for combating infectious diseases. In this study, we determined the efficacy of Cefixime and its novel magnetic iron oxide formulation, Sulfamethoxazole, Moxifloxacin, and their silica-based nanoconjugates against MDR bacteria. Here, for the first time, we synthesized, characterized and tested these novel formulations.

Cefixime is very effective against streptococci such as *S. pneumoniae* and *S. pyogenes*, having moderate activity against *S. aureus* while ineffective against Gram-negative *P. aeruginosa* [20]. In this study, we evaluated the antibacterial activity of Cefixime against a panel of Gram-positive and Gram-negative bacteria. Cefixime revealed significant antibacterial activity against *S. pneumoniae, B. cereus, S. pyogenes*, and MRSA. Upon conjugation with CA-MNPs, this activity was exceptionally enhanced against *S. pneumoniae, S. pyogenes*, and MRSA but not against *B. cereus*. The MIC and MBC of Cefixime were found to be 6.25 µg/mL and 12.5 µg/mL for *E. coli* K1 and >200 µg/mL MIC was recorded against MRSA. However, upon conjugation, MIC and MBC was significantly reduced to 12.5 µg/mL

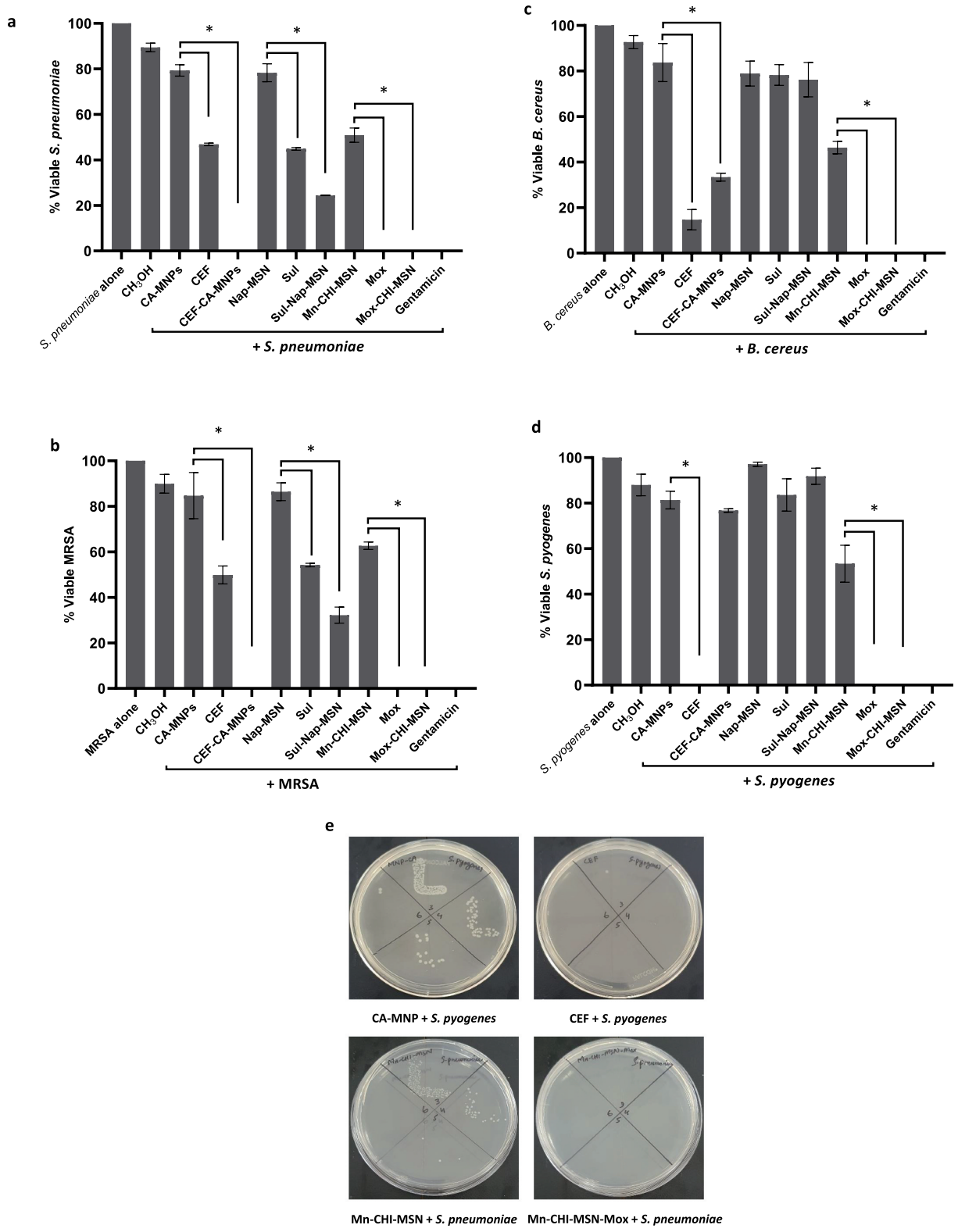

Figure 7. Magnetic iron oxide and silica based NPs loaded with different drugs eradicated Gram-positive pathogenic bacteria. Briefly, NPs and drug conjugates were mixed with test bacteria at 37°C for 2 h. After this, cultures were serially diluted and plated on nutrient agar plates. The plates were incubated for overnight at 37°C and subsequently viable bacteria were counted. For controls, bacteria incubated alone in PBS and with gentamicin (100 µg/mL) was used as negative and positive controls, respectively. The data are expressed as the means ± standard errors from several independent experiments performed in duplicate where (*) represent when $P \leq 0.05$.

and 25 µg/mL respectively but in case of *E. coli* K1 after conjugation the Cefixime lost its activity. Our results are in agreement with Ali et al., (2020), who evaluated the antibacterial activity of Cefixime alone as well as in conjugation with AgNPs and AuNPs against *S. aureus* [20]. Similarly, in a recent study, Cefixime was tested alone and in combination with Ag, Ni, Cu, and ZnO NPs against *S. typhi* and *S. paratyphi*. Cefixime in

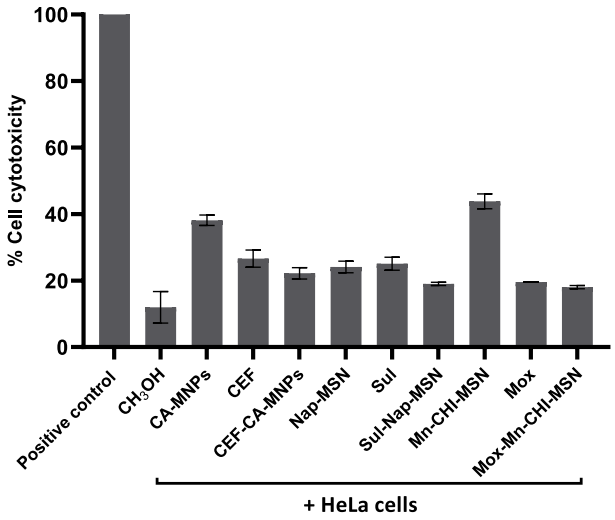

Figure 8. Magnetic iron oxide and silica based NPs loaded with different drugs revealed negligible cytotoxic effects against HeLa cell lines. Human cells were grown in 96 well plate up to 80–90% confluency as discussed in material and methods. Next, cells monolayer was challenged with NPs, drugs and drugs-NPs combinations for 24 h at 37°C in humidified conditions with 5% CO_2. Cells alone in RPMI was taken as negative control. The data are presented as mean ± standard error of three times independent experiments performed in duplicates. Data was analyzed using Graph Pad Prism software (8.0.2).

combination with NPs showed noteworthy antibacterial effects against the test bacteria [28]. Polyether sulfone membrane containing AgNPs drastically reduced *E. coli* growth [62]. NPs produced biosynthetically by *P. aeruginosa* could also be used for biomineralization and heavy metal transformation [63]. Cinnamic acid gold NPs showed amazing antibacterial effects against *E. coli* K1 and MRSA [64]. Rini et al., (2020) reported MIC and MBC values against *S. enterica* as 32 µg/mL and 64 µg/mL [65].

Moxifloxacin revealed exceptional antibacterial activity against both Gram-positive and Gram-negative bacteria. Moxifloxacin alone as well as in the combination with silica-based NPs showed 100% killing effects against all Gram-positive isolates. Our results are in agreement with the previous literature for example; triple-component nanocomposite i.e. Mox loaded with chitosan-silver-sericin films showed promising antibacterial activity against *P. aeruginosa, S. aureus*, and MRSA [26]. Similarly, the conjugation of Moxifloxacin with metallic NPs (Au) and (Ag) revealed amazing antibacterial activity against *B. subtilis, E. coli, S. aureus, Streptococcus features*, and *P. aeruginosa* [23]. Lalitha et al., (2012) reported the MIC_{50} and MIC_{90} of Mox against *S. aureus* that was equal to 1 µg/mL and 8 µg/mL, respectively, [66]. Balfour and Lamb, (2000) identified the MIC_{90} in the range of 2 to 8 mg/L, which quite higher as compared to our study [67]. Our synthesized nanocomposite formulations showed great potency as the test bacteria in our study was MRSA (MDR clinical isolate). Conjugation further boosted the bactericidal activity lowered the MIC and MBC values for *E. coli* K1 and MRSA to *i.e.* 3.125 µg/mL and 6.25 µg/mL in comparison to MIC and MBC of Moxifloxacin alone which was 6.25 µg/mL and 12.5 µg/mL for *E. coli* K1, and 12.5 µg/mL and 25 µg/mL for MRSA, respectively. In another study, MIC_{50} and MBC_{50} of Mox were identified against Penicillin-sensitive, Penicillin-intermediately resistant, Penicillin-resistant and Macrolide-resistant *S. pneumoniae*. The MIC_{50} values were recorded as 30 µg/mL, 60 µg/mL, 60 µg/mL, and 30 µg/mL respectively, while MBC_{50} values were 60 µg/mL, 120 µg/mL, 60 µg/mL, and 60 µg/mL respectively [68]. The antibiotic Mox inhibit bacterial DNA gyrase and topoisomerase IV that can be reversed by a single genetic mutation [67]. The mechanism of action of these synthesized Moxifloxacin-based nano-formulations are likely similar but that needs to be determined in future studies.

Sulfamethoxazole showed important antibacterial activity only in case of *S. pneumoniae* and MRSA but failed to reduce the bacterial population for all other bacteria tested. Our results are in contradiction with a recent study where Sulfamethoxazole showed obvious antibacterial activity against *E. coli* [21] whereas in our study the antibiotic did not show any effects. This could be due to the fact that the K1 strain was utilized in our study and is more resistant to antibiotics [69]. However, conjugation with silica- based NPs improved its antibacterial effects and showed significant bactericidal activity against *P. aeruginosa, S. marcescens, S. pneumoniae*, and MRSA. Rostamizadeh et al., (2019) reported that upon conjugation with metal complex Sulfamethoxazole presented important antibacterial properties against *S. aureus* and *E. coli* [21].

Antimicrobial properties of magnetic iron oxide nanoparticles have been widely documented. Their antibacterial potential is due to the generation of reactive oxygen species, which damage bacteria's outer membrane [70]. The antimicrobial activity can also be modulated by varying surface ligands, which is also an aspect of bactericidal potential of iron oxide nanoparticles [37]. Similarly, mesoporous silica nanoparticles are well reported as hydrophobic drug carrier due to available pores within nanostructures. Surface functionalization with groups having antibacterial potential has been reported to enhance the antimicrobial potential of loaded drugs [71]. Therefore, the current approach was hypothesized by functionalizing antibacterial agents on the surface of silica nanoparticles that are able to enhance the overall antimicrobial activity of drug-loaded nanoformulations.

Of note, magnetic iron oxide NPs, Silica-based NPs, and drug-loaded NPs presented minor cytotoxic effects on human cell lines. Our findings are consistent

with previously published data. For example, Iqbal et al., (2021) reported that Moxifloxacin loaded NPs showed biological activity with no cytotoxic effects toward Caco-2 cell line [48]. Similarly, Hesperidin and Naringin-based green synthesized NPs exhibited strong antimicrobial activity with minimal cytotoxicity toward HeLa cell lines [13]. In another study, ZnO-NPs revealed remarkable antibacterial activity with minor cytotoxicity against human cells [72]. In future, analytical methods are required to reliably perceive and characterize such novel nanocomposites as well as to investigate their antibacterial activity and their possible mechanism of action.

5. Conclusion

It is anticipated that such novel nanocomposites formulations can be utilized to treat MDR infections in the clinical setting and should be tested with other antibiotics to enhance their efficacy, against other microorganisms, such as viruses, amoebae, and fungi. Moreover, it is necessary to test these novel nanoformulations *in vivo* studies as well as in clinical studies.

Disclosure statement

No potential conflict of interest was reported by the author(s).

Funding

This research was funded by the American University of Sharjah and University of Sharjah;American University of Sharjah

ORCID

Naveed Ahmed Khan http://orcid.org/0000-0001-7667-8553
Ruqaiyyah Siddiqui http://orcid.org/0000-0001-9646-6208

Ethical approval and consent to participate

This article does not contain any studies with human participants. This article does not contain any studies involving animals.

References

[1] Brennan-Krohn T, Manetsch R, O'Doherty GA, et al. New strategies and structural considerations in development of therapeutics for carbapenem-resistant *Enterobacteriaceae*. Transl Res. 2020;220:14–32.
[2] Mandal SM, Roy A, Ghosh AK, et al. Challenges and future prospects of antibiotic therapy: from peptides to phages utilization. Front Pharmacol. 2014;5:105.
[3] Farha MA, Brown ED. Drug repurposing for antimicrobial discovery. Nat Microbiol. 2019;4(4):565–577.
[4] Odonkor ST, Addo KK. Bacteria resistance to antibiotics: recent trends and challenges. Int J Biol Med Res. 2011;2(4):1204–1210.
[5] Ansari MJ, Al-Ghamdi A, Usmani S, et al. *In vitro* evaluation of the effects of some plant essential oils on *Ascosphaera apis*, the causative agent of Chalkbrood disease. Saudi J Biol Sci. 2017;24(5):1001–1006.
[6] Meo SA, Al-Asiri SA, Mahesar AL, et al. Role of honey in modern medicine. Saudi J Biol Sci. 2017;24(5):975–978.
[7] Akova M. Epidemiology of antimicrobial resistance in bloodstream infections. Virulence. 2016;7(3):252–266.
[8] Frieri M, Kumar K, Boutin A. Antibiotic resistance. J Infect Public Health. 2017;10(4):369–378.
[9] Akbar N, Khan NA, Sagathevan K, et al. Gut bacteria of *Cuora amboinensis* (turtle) produce broad-spectrum antibacterial molecules. Sci Rep. 2019a;9(1):1–19.
[10] Akbar N, Siddiqui R, Sagathevan K, et al. Gut bacteria of water monitor lizard (*Varanus salvator*) are a potential source of antibacterial compound (s). Antibiotics. 2019b;8(4):164.
[11] Khan NA, Siddiqui R, Elsheikha H. Enemy within: strategies to kill'superbugs' in hospitals. Int J Antimicrob Agents. 2010;36(3):291.
[12] Siddiqui R, Khan NA. Infection control strategy by killing drug-resistant bacteria. Pathog Glob Health. 2013;107(5):215.
[13] Anwar A, Masri A, Rao K, et al. Antimicrobial activities of green synthesized gums-stabilized nanoparticles loaded with flavonoids. Sci Rep. 2019;9(1):1–12.
[14] Bodey GP, Bolivar R, Fainstein V, et al. Infections caused by *Pseudomonas aeruginosa*. Rev Infect Dis. 1983;5(2):279–313.
[15] Recio R, Mancheño M, Viedma E, et al. Predictors of mortality in bloodstream infections caused by Pseudomonas aeruginosa and impact of antimicrobial resistance and bacterial virulence. Antimicrob Agents Chemother. 2020;64(2):e01759–19.
[16] Khanna A, Khanna M, Aggarwal A. *Serratia marcescens*-a rare opportunistic nosocomial pathogen and measures to limit its spread in hospitalized patients. J Clin Diagn Res. 2013;7(2):243.
[17] Vading M, Nauclér P, Kalin M, et al. Invasive infection caused by *Klebsiella pneumoniae* is a disease affecting patients with high comorbidity and associated with high long-term mortality. PloS One. 2018;13(4):e0195258.
[18] Silva-Costa C, Brito MJ, Pinho MD, et al., Portuguese Group for the Study of Streptococcal Infections. Pediatric complicated pneumonia caused by *Streptococcus pneumoniae* serotype 3 in 13-valent pneumococcal conjugate vaccines, Portugal, 2010–2015. Emerg Infect Dis. 2018;24(7):1307.
[19] Brogden RN, Campoli-Richards DM. Cefixime. Drugs. 1989;38(4):524–550.
[20] Ali S, Perveen S, Shah MR, et al. Bactericidal potentials of silver and gold nanoparticles stabilized with cefixime: a strategy against antibiotic-resistant bacteria. J Nanopart Res. 2020;22(7):1–12.
[21] Rostamizadeh S, Daneshfar Z, Moghimi H. Synthesis of sulfamethoxazole and sulfabenzamide metal complexes; evaluation of their antibacterial activity. Eur J Med Chem. 2019;171:364–371.
[22] Sahyon HA, Ramadan EN, Mashaly MM. Synergistic effect of quercetin in combination with sulfamethoxazole as new antibacterial agent: *in vitro* and in vivo study. Pharm Chem J. 2019;53(9):803–813.

[23] Seku K, Yamala AK, Kancherla M, et al. Synthesis of moxifloxacin–Au (III) and Ag (I) metal complexes and their biological activities. J Anal Sci Technol. 2018;9(1):1–13.
[24] Masri A, Anwar A, Khan NA, et al. The use of nanomedicine for targeted therapy against bacterial infections. Antibiotics. 2019;8(4):260.
[25] Shah A, Yameen MA, Fatima N, et al. Chemical synthesis of chitosan/silver nanocomposites films loaded with moxifloxacin: their characterization and potential antibacterial activity. Int J Pharm. 2019a;561:19–34.
[26] Shah A, Buabeid MA, Arafa ESA, et al. The wound healing and antibacterial potential of triple-component nanocomposite (chitosan-silver-sericin) films loaded with moxifloxacin. Int J Pharm. 2019b;564:22–38.
[27] Ali R, Batool T, Manzoor B, et al. Nanobiotechnology-based drug delivery strategy as a potential weapon against multiple drug-resistant pathogens. In: Antibiotics and antimicrobial resistance genes in the environment. Elsevier; 2020. p. 350–368.
[28] Kapadia C, Alhazmi A, Patel N, et al. Nanoparticles combined with cefixime as an effective synergistic strategy against *Salmonella enterica typhi*. Saudi J Biol Sci. 2021;28(8):4164–4172.
[29] Zakeri Z, Allafchian A, Vahabi MR, et al. Synthesis and characterization of antibacterial silver nanoparticles using essential oils of crown imperial leaves, bulbs and petals. Micro Nano Lett. 2021;16(11):533–539.
[30] Allafchian A, Mousavi SH, Jalali SAH. Synthesis of antibacterial flower-like silver nanostructures by self-assembly of diphenylalanine peptide on graphite. Micro Nano Lett. 2020;15(7):486–489.
[31] Askari Z, Vahabi MR, Allafchian A, et al. Biosynthesis of antibacterial silver nanoparticles using *Astragalus verus* Olivier. Micro Nano Lett. 2020;15(2):66–71.
[32] Kawish M, Jabri T, Elhissi A, et al. Galactosylated iron oxide nanoparticles for enhancing oral bioavailability of ceftriaxone. Pharm Dev Technol. 2021;26(3):291–301.
[33] Vazquez NI, Gonzalez Z, Ferrari B, et al. Synthesis of mesoporous silica nanoparticles by sol–gel as nanocontainer for future drug delivery applications. Boletín de la Sociedad Española de Cerámica y Vidrio. 2017;56(3):139–145
[34] Chaubey P, Patel RR, Mishra B. Development and optimization of curcumin-loaded mannosylated chitosan nanoparticles using response surface methodology in the treatment of visceral leishmaniasis. Expert Opin Drug Deliv. 2014;11(8):1163–1181.
[35] Date AA, Nagarsenker MS, Patere S, et al. Lecithin-based novel cationic nanocarriers (Leciplex) II: improving therapeutic efficacy of quercetin on oral administration. Mol Pharm. 2011;8(3):716–726.
[36] Katara R, Sachdeva S, Majumdar DK. Design, characterization, and evaluation of aceclofenac-loaded Eudragit RS 100 nanoparticulate system for ocular delivery. Pharm Dev Technol. 2019;24(3):368–379.
[37] Abdelnasir S, Anwar A, Kawish M, et al. Metronidazole conjugated magnetic nanoparticles loaded with amphotericin B exhibited potent effects against pathogenic *Acanthamoeba castellanii* belonging to the T4 genotype. AMB Express. 2020;10(1):1–11.
[38] Akbar N, Siddiqui R, Iqbal M, et al. Gut bacteria of cockroaches are a potential source of antibacterial compound (s). Lett Appl Microbiol. 2018;66(5):416–426.
[39] Akbar N, Siddiqui R, Iqbal M, et al. Gut bacteria of *Rattus rattus* (Rat) produce broad-spectrum antibacterial lipopeptides. ACS Omega. 2021;6(18):12261–12273.
[40] Akbar N, Siddiqui R, Iqbal M, et al. Antibacterial activities of selected pure compounds isolated from gut bacteria of animals living in polluted environments. Antibiotics. 2020;9(4):190.
[41] Parvekar P, Palaskar J, Metgud S, et al. The minimum inhibitory concentration (MIC) and minimum bactericidal concentration (MBC) of silver nanoparticles against *Staphylococcus aureus*. Biomater Invest Dent. 2020;7(1):105–109
[42] Kawish M, Elhissi A, Jabri T, et al. Enhancement in oral absorption of ceftriaxone by highly functionalized magnetic iron oxide nanoparticles. Pharmaceutics. 2020;12(6):492.
[43] Costa VM, de Souza MCM, Fechine PBA, et al. Nanobiocatalytic systems based on lipase-Fe3O4 and conventional systems for isoniazid synthesis: a comparative study. Braz J Chem Eng. 2016;33(3):661–673.
[44] Hachani R, Lowdell M, Birchall M, et al. Polyol synthesis, functionalisation, and biocompatibility studies of superparamagnetic iron oxide nanoparticles as potential MRI contrast agents. Nanoscale. 2016;8(6):3278–3287.
[45] Tripathi IP, Gupta P, Gupta M, et al. Characterization and validation of cefixime trihydrate tablets with ftir and Rp-Hplc Techeniques. Indian J Appl Res. 2015;5(4):691.
[46] Oliveira LFD, Bouchmella K, Picco AS, et al. Tailored silica nanoparticles surface to increase drug load and enhance bactericidal response. J Braz Chem Soc. 2017;28:1715–1724.
[47] Mehrabi F, Shamspur T, Mostafavi A, et al. Inclusion of sulfamethoxazole in a novel $CuFe_2O_4$ nanoparticles/mesoporous silica-based nanocomposite: release kinetics and antibacterial activity. Appl Organomet Chem. 2021;35(1):e6035.
[48] Iqbal O, Shah S, Abbas G, et al. Moxifloxacin loaded nanoparticles of disulfide bridged thiolated chitosan-eudragit RS100 for controlled drug delivery. Int J Biol Macromol. 2021;182:2087–2096.
[49] Gutiérrez L, De La Cueva L, Moros M, et al. Aggregation effects on the magnetic properties of iron oxide colloids. Nanotechnology. 2019;30(11):112001.
[50] Stewart M, Bartholomew B, Currie F, et al. Pyranoisoflavones from Rinorea welwitschii. Fitoterapia. 2000;71(5):595–597.
[51] Kong ZL, Kuo HP, Johnson A, et al. Curcumin-loaded mesoporous silica nanoparticles markedly enhanced cytotoxicity in hepatocellular carcinoma cells. Int J Mol Sci. 2019;20(12):2918.
[52] Imran M, Shah MR, Ullah F, et al. Glycoside-based niosomal nanocarrier for enhanced in-vivo performance of Cefixime. Int J Pharm. 2016;505(1–2):122–132.
[53] Han C, Huang H, Dong Y, et al. A comparative study of the use of mesoporous carbon and mesoporous silica as drug carriers for oral delivery of the water-insoluble drug carvedilol. Molecules. 2019;24(9):1770.
[54] Juère E, Florek J, Bouchoucha M, et al. *In vitro* dissolution, cellular membrane permeability, and anti-inflammatory response of resveratrol-encapsulated mesoporous silica nanoparticles. Mol Pharm. 2017;14(12):4431–4441.

[55] Kaasalainen M, Aseyev V, Von Haartman E, et al. Size, stability, and porosity of mesoporous nanoparticles characterized with light scattering. Nanoscale Res Lett. 2017;12(1):1–10.
[56] Kanwal T, Saifullah S, Ur Rehman J, et al. Design of absorption enhancer containing self-nanoemulsifying drug delivery system (SNEDDS) for curcumin improved anti-cancer activity and oral bioavailability. J Mol Liq. 2021;324:114774.
[57] Mohammed MA, Syeda J, Wasan KM, et al. An overview of chitosan nanoparticles and its application in non-parenteral drug delivery. Pharmaceutics. 2017;9 (4):53.
[58] Ventola CL. The antibiotic resistance crisis: part 1: causes and threats. Pharm Ther. 2015;40(4):277.
[59] Gould IM, Bal AM. New antibiotic agents in the pipeline and how they can help overcome microbial resistance. Virulence. 2013;4(2):185–191.
[60] Sengupta S, Chattopadhyay MK, Grossart HP. The multifaceted roles of antibiotics and antibiotic resistance in nature. Front Microbiol. 2013;4:47.
[61] Wright GD. Something old, something new: revisiting natural products in antibiotic drug discovery. Can J Microbiol. 2014;60(3):147–154.
[62] Rana S, Nazar U, Ali J, et al. Improved antifouling potential of polyether sulfone polymeric membrane containing silver nanoparticles: self-cleaning membranes. Environ Technol. 2018;39 (11):1413–1421.
[63] Ali J, Ali N, Jamil SUU, et al. Insight into eco-friendly fabrication of silver nanoparticles by *Pseudomonas aeruginosa* and its potential impacts. J Environ Chem Eng. 2017;5(4):3266–3272.
[64] Anwar A, Siddiqui R, Shah MR, et al. Gold nanoparticle-conjugated cinnamic acid exhibits antiacanthamoebic and antibacterial properties. Antimicrob Agents Chemother. 2018;62(9):e00630–18.
[65] Rini IJ, Islam MA, Ahsan S. Effect of selected antibiotics on biofilm formed by *Salmonella enterica serovars Typhi* and *Paratyphi*. Bangladesh J Microbiol. 2020;37(2):62–65
[66] Lalitha P, Srinivasan M, Manikandan P, et al. Relationship of in vitro susceptibility to moxifloxacin and in vivo clinical outcome in bacterial keratitis. Clinl Infect Dis. 2012;54(10):1381–1387.
[67] Balfour JAB, Lamb HM. Moxifloxacin. Drugs. 2000;59 (1):115–139.
[68] Klugman KP, Capper T. Concentration-dependent killing of antibiotic-resistant pneumococci by the methoxyquinolone moxifloxacin. J Antimicrob Chemother. 1997;40(6):797–802.
[69] Jankowski S, Franiczek R. Susceptibility of *Escherichia coli* with capsular antigen K1 isolated from urinary tract infection on the joint action of cefotaxime and normal human serum. Nephron. 1994;68(4):519–520.
[70] Arakha M, Pal S, Samantarrai D, et al. Antimicrobial activity of iron oxide nanoparticle upon modulation of nanoparticle-bacteria interface. Sci Rep. 2015;5(1):1–12.
[71] Michailidis M, Sorzabal-Bellido I, Adamidou EA, et al. Modified mesoporous silica nanoparticles with a dual synergetic antibacterial effect. ACS Appl Mater Interfaces. 2017;9(44):38364–38372.
[72] Colon G, Ward BC, Webster. TJ. Increased osteoblast and decreased *Staphylococcus epidermidis* functions on nanophase ZnO and TiO_2. J Biomed Mater Res A. 2006;78A(3):595–604.